Lawrence Berkeley National Laboratory
Lawrence Berkeley National Laboratory

Title
Negative Electrodes for Li-Ion Batteries

Permalink
https://escholarship.org/uc/item/4sv7n3f0

Authors
Kinoshita, Kim
Zaghib, Karim

Publication Date
2001-10-01

Peer reviewed

Negative Electrodes for Li-Ion Batteries

Kim Kinoshita[a] and Karim Zaghib[b]

[a]Lawrence Berkeley National Laboratory, 1 Cyclotron Road, Berkeley, CA, 94720, USA

[b]Institut de Recherche d'Hydro-Québec, 1800 boul, Lionel-Boulet, Varennes, Québec, J3X 1S1, Canada

Abstract

Graphitized carbons have played a key role in the successful commercialization of Li-ion batteries. The physicochemical properties of carbon cover a wide range; therefore identifying the optimum active electrode material can be time consuming. The significant physical properties of negative electrodes for Li-ion batteries are summarized, and the relationship of these properties to their electrochemical performance in nonaqueous electrolytes, are discussed in this paper.

Keywords: carbon, lithium intercalation, reversible capacity, irreversible capacity

Introduction

Sony Corporation was the first to commercialize Li-ion batteries for portable electronic devices in the early 1990's. Since that time, the number of companies producing Li-ion batteries has proliferated. Three major markets for these batteries are cellular phones, laptop computers and video cameras. Manufacture of large-scale Li-ion batteries for transportation applications in electric vehicles (EVs) and hybrid electric vehicles (HEVs) has lagged further behind the consumer market.

The active materials in the electrodes of commercial Li-ion batteries are usually graphitized carbons in the negative electrode and $LiCoO_2$ in the positive electrode. The electrolyte contains $LiPF_6$ and solvents that consist of mixtures of cyclic and linear carbonates. Electrochemical intercalation is difficult with graphitized carbon in $LiClO_4$/propylene carbonate (PC) because of rapid electrolyte decomposition and exfoliation of the crystallite structure. Successful intercalation of Li^e ions into graphite was made possible by using a mixed solvent electrolyte system such as $LiPF_6$ in ethylene carbonate (EC) + diethyl carbonate (DEC). On the other hand, $LiClO_4$ in PC is an acceptable electrolyte for intercalation of Li^+ ions in nongraphitized carbons such as petroleum coke, but the electrochemical Li capacity is less, amounting to about 180 mAh/g C. Other amorphous carbons have been investigated, and some have electrochemical capacities that exceed 372 mAh/g C, which is the capacity of graphite.

For transportation applications, safety, cost and calendar life are key technical issues that must be resolved. One approach to understanding and resolving these issues is to utilize mathematical models that can guide experimentalists in their development efforts to identify improved electrode components. The discussion in this paper is

directed at the electrochemical performance of negative electrodes for Li-ion batteries that could benefit from mathematical models. The physicochemical properties and the electrochemical performance of active materials in the negative electrodes are intimately connected, therefore both must be considered in a viable model. With this in mind, the significant physical properties of negative electrodes for Li-ion batteries are summarized, and the relationship of these properties to their electrochemical performance in nonaqueous electrolytes, are discussed.

Physicochemical Properties

Elemental carbon is found in three major crystallographic structures: (i) diamond, (ii) buckminsterfullerene and (iii) graphite. Diamond has a tetrahedral structure with covalent bonds (sp^3-hybridization). Buckminsterfullerene ("fullerene") in its common form, C_{60}, resembles a soccer ball consisting of carbon atoms in pentagonal and hexagonal arrays. The graphite structure consists of carbon atoms arranged in hexagonal rings that are stacked in an orderly fashion (see Figure 1). Only weak van der Waals bonds exist between these layer planes. The usual stacking sequence of the carbon layers is ABABA... for hexagonal graphite. The stacking sequence ABCABC... is found less frequently (i.e., usually a few percent) and is called rhombohedral graphite. The d(002) interplanar spacing in graphite is 0.3354 nm in the c-axis direction (perpendicular to the layer planes), while the C-C bond distance in the a-axis direction (parallel to the layer planes) is 0.142 nm, slightly longer than those in benzene, 0.139 nm. Graphite has two distinct surfaces, the basal plane and the edge sites. Furthermore, the physical properties of graphite are highly anisotropic because of this crystallographic structure. For instance, the electrical conductivity in the direction parallel to the basal plane is about 100 times higher than in the perpendicular direction.

Amorphous carbons also consist of hexagonal carbon rings, but the number of these rings that constitutes a crystallite is much less that that for graphite. In addition there is very little order between the layers. Instead, the layers are rotated with respect to each other but parallel to each other (referred to as turbostratic). i.e., no three-dimensional ordering. The layer spacing of carbon blacks is typically >0.350 nm, and the crystallite sizes are typically 1.0 nm to 2.0 nm for L_a (crystallite size in the direction parallel to the basal plane) and L_c (crystallite size in the direction perpendicular to the basal plane). On the other hand, L_a and L_c for graphites can be >100 nm. The surface area of graphite and amorphous carbon can be <10 m^2/g to >1000 m^2/g, respectively. The diameter of carbonaceous materials such as carbon fibers is typically 10 μm. Graphite powders are available with average particle size of 10-100 μm, and those in the lower range of particle size are used in Li-ion batteries. The densities of these carbonaceous materials are 2.25 g/cm^3 for graphite and usually <1.80 g/cm^3 for amorphous carbon. Further details on the physical properties can be found in various review articles (1-5).

Carbon is truly a unique material with physicochemical properties that vary from the extremes of graphite to highly amorphous carbon. These carbons have varying degrees of long- and short-range order, different bonding between the carbon atoms, different crystalline structures, and also of importance in electrochemistry, they possess a wide range of chemical properties. The surface of carbonaceous materials contains

numerous chemical complexes that are formed during the manufacturing step by oxidation or introduced during post-treatment. The surface complexes are typically chemisorbed oxygen groups such as carbonyl, carboxyl, lactone, quinone and phenol. Carbon-hydrogen bonds are also present, particularly in carbonaceous materials obtained by carbonizing polymers at low temperatures, typically <1000˚C. These surface groups exhibit different thermal stabilities, with the functional groups that contain two oxygen atoms (carboxyl and lactone) desorbing as CO_2 at generally <500˚C. Functional groups that contain one oxygen atom (phenol, quinone) evolve CO at temperatures of about 600˚C and higher. Analysis of carbon blacks indicates that the hydrogen content is in the range 0.01% to 0.7%. The hydrogen that is bonded to carbon is relatively stable, commencing evolution at about 700˚C and reaching a maximum at about 1100˚C. Other common heteroatoms such as nitrogen and sulfur are also found in carbon. In the case of nitrogen, it is usually present in minor amounts. On the other hand, sulfur can be present in high concentrations, >1%, depending on the precursor that is used to manufacture the carbonaceous material. Besides sulfur that is bonded to carbon, other forms such as elemental sulfur, inorganic sulfate and organosulfur compounds may be present. The carbon-sulfur surface compounds on carbon blacks are relatively stable, but they desorb as H_2S when carbon is heat treated in H_2 between 500˚ and 1000˚C.

Carbons are generally classified as "soft carbon" (graphitizable) or "hard carbon" (non-graphitizable). Examples of soft carbon are petroleum coke and carbon black, and examples of hard carbons are glassy carbon and activated carbon. The physicochemical properties of soft carbons are amenable to change by heat treatment in an inert environment.
The graphitizaton of soft carbons is quantified by the term "degree of graphitization" (g) which is correlated to the d(002) spacing (6):

$$g = [d(002) - 3.44]/[-0.086] \qquad [1]$$

For ideal graphite with d(002) = 0.3354 nm, g = 1; and for amorphous carbon with d(002) = 0.344 nm, g = 0. In this definition, a d(002) spacing of 0.344 nm distinguishes a carbon with random orientation of layer planes (turbostratic) and no notable three-dimensional ordering.

Electrochemical Performance Parameters

In Li-ion batteries, carbon particles are used in the negative electrode as the host for Li^+-ion intercalation (or storage), and carbon is also utilized in the positive electrode to enhance its electronic conductivity. Graphitized carbons are probably the most common crystalline structure of carbon used in Li-ion batteries. Reviews of carbon technology relevant to negative electrodes for Li-ion batteries are presented by Megahed and Scrosati (7), Besenhard (7), Tarascon and Guyomard (9), Houssain (10), Kinoshita (11) and Endo (12). The following discussion is directed at carbon in the negative electrode of Li-ion batteries, and the role of carbon in the positive electrode is outside the scope of this paper.

The electrochemical reaction at the negative electrode in Li-ion batteries is represented by

$$xLi^+ + 6C + xe^- \rightarrow Li_xC_6$$
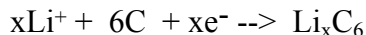
The Li^+ ions in the electrolyte enter between the layer planes of graphite during charge (intercalation). The distance between the graphite layer planes expands by about 10% to accommodate the Li^+ ions. When the cell is discharged (de-intercalation), Li^+ ions are removed from the graphite structure and return to the electrolyte. The maximum amount of Li^+ ions that is stored in graphite is equivalent to x = 1 (LiC_6). Other carbons have been used which yield values of x that may be greater or less than one. A schematic representation of the potential profiles for carbon electrodes when Li^+ ions are intercalated at constant current is illustrated in Figure 2. In the case of highly graphitized carbon, the potential initially drops rapidly to near 0.8 V (*vs.* Li/Li^+) before electrolyte decomposition and the formation of a surface film occur. When these reactions take place, the potential remains close to a constant value. The duration of the potential plateau varies with the extent of electrolyte decomposition. Following electrolyte decomposition, the potential declines and the majority of Li^+ ion intercalation occurs at <0.25 V. With highly graphitized carbons, inflections and plateaus in the potential-composition (x) profiles are evident which are related to staging phenomena. Amorphous carbons exhibit a sloping profile, with no evidence of staging. In the extreme case, electrolyte decomposition and gas evolution can occur with little or no Li intercalation. The first charge half-cycle of carbon (Q_t) in a Li-ion cell involves Li insertion or storage in the carbon structure (Q_{in}) and electrolyte decomposition (Q_{irr}). The subsequent discharge half-cycle leads to de-intercalation of Li^+ ions (Q_{dein}) and minimal further electrolyte decomposition. The difference between the charge and discharge half-cycles ($Q_{irr} = Q_t - Q_{dein}$) is attributed to the "irreversible capacity loss" (ICL), which represents the charge (coulombs) associated with electrolyte decomposition. In subsequent charge/discharge cycles, the charge capacity with a useful carbonaceous material approaches Q_{in}, which is approximately constant with cycling and is identified with the reversible Li storage capacity ($Q_{in} = Q_{rev}$).

The magnitude of the reversible Li storage capacity (Q_{rev}) is strongly dependent on many parameters, including the physical properties of the carbon, electrolyte composition, current density and the potential range over which intercalation/deintercalation occurs. A simplified relationship between the crystallographic structure of carbon, as represented by d(002) spacing, and its reversible Li storage capacity has been proposed (13-15). Published data for Q_{rev} obtained with various carbonaceous materials, ranging from highly ordered graphite to highly disordered carbon, are plotted as a function of their d(002) spacing in Figure 3. In this plot, no attempt was made to differentiate between the methods used to obtain Q_{rev}. Furthermore, the plot does not indicate the source of the data, but different symbols are used to indicate the various sources that are cited. It should be noted that data from many of the major research organizations that have published results for Q_{rev} are included in the plot. A solid line is shown on the plot to illustrate a trend in Q_{rev} as a function of the d(002) spacing. Based on this line, there appears to be a minimum in Q_{rev} at a d(002) spacing of approximately 0.344 nm. Perhaps coincidentally, the degree of graphitization G is equal to zero at d(002) = 0.344 nm, as indicated above. For d(002) of

4

0.344 nm--> 0.3354 nm, G changes from 0 --> 1(denoted by the dashed line). Taking the result in Figure 3, and the degree of graphitization, we suggest that the ability of carbonaceous materials to intercalate Lie decreases as G --> 0 and d (002) --> 0.344 nm because the structure becomes turbostratic. However, for d(002) > 0.344 nm, the crystallite domains L_a and L_c become smaller, microcavities are present, and the probability of forming single graphene planes increase. Under these conditions, classical Li intercalation is unlikely. Instead other mechanisms (16-27) are proposed to explain the experimental results at higher d(002) spacing in Figure 3.

The parabolic relationship illustrated by the solid line in Figure 3 has been analyzed by Flandrois and Simon (28). They described the relationship by the equation

$$x = (1 - g)^2 x_{\alpha\alpha} + 2g(1 - g)x_{\alpha\beta} + g^2 \qquad [2]$$

where $x_{\alpha\alpha}$ and $x_{\alpha\beta}$ are the contributions to x (in $Li_x C_6$) from different sites in the carbon structure. The β state refers to the layer planes in a perfect graphite structure, and α refers to layer planes that contain interstitial atoms. This distinction suggests a crystallinity that ranges from graphite to amorphous or disordered carbon, respectively. Thus, in partially graphitized carbon, there may exist interlayer spacings of $\beta\beta$, $\alpha\beta$ and $\alpha\alpha$. Flandrois and Simon (28) found that Equation [2] with $x_{\alpha\alpha} = 0.75$ and $x_{\alpha\beta} = 0.20$ showed good agreement with their experimental data. Fujimoto et al. (29) derived the following expression

$$C/Li = 6 (1+ d_{002}/L_c) (1+ 2d_{c\text{-}c}[\sqrt{3}L_a + d_{c\text{-}c}]/[L_a^2 + d_{c\text{-}c}^2]) \quad [3]$$

that relates the reversible capacity to crystallographic parameters of carbon, i.e., d(002) spacing, crystallite size in parallel (L_a) and perpendicular (L_c) to the basal plane, and the carbon-carbon bond length ($d_{c\text{-}c} = 0.142$ nm) in the layer planes. In the limit where L_a and L_c are large (i.e., ≥100 nm), C/Li = 6 (x = 1) in Equation [3], which is typical for graphite.

A linear relationship between Q_{rev} and Q_{irr},

$$Q_{rev} = 381 - 0.73Q_{irr} \qquad [4]$$

was observed with natural and artificial graphites in $LiPF_6$ in EC-DMC-DME (1:1:2) by Yazami (30). This linear dependence was tentatively assigned to a diffusion model. Analysis of Q_{rev} obtained with natural graphite in 1 M $LiClO_4$/1:1 (volume ratio) ethylene carbonate (EC) - dimethyl carbonate (DMC) in our laboratory did not show a linear dependence (see Figure 4). Analysis of other published results for Q_{rev} and Q_{irr} also showed no relationship such as that given by Equation [4]. No plausible explanation for this discrepancy is available at this time. However, it should be noted that Yazami suggested that Equation [4] is probably specific to his experimental conditions (i.e., graphitic carbon, temperature, electrolyte composition, cycling rate and voltage limits).

There is good agreement on the relationship between Q_{irr} and the BET surface area (S_{BET}) of carbon. The data obtained with natural graphite (see Figure 5A) in $LiClO_4$ in EC-DMC (1:1) show a linear relationship that can be expressed by the equation

5

$$Q_{irr} = 7.13 + 7.10S_{BET} \qquad [5]$$

Joho et al. (31) also observed a linear correlation with artificial graphite in LiPF$_6$ in EC-DMC (1:1), and the results were fitted to an equation given by

$$Q_{irr} = 2.55 \; C \; 1.18S_{BET} \qquad [6]$$

The plot in Figure 5B is a compilation of a variety of carbons from an analysis by Tran et al. (32) which further supports the trend indicating that Q_{irr} increases with an increase in the surface area of the carbon electrode.

Graphitized carbon consists of basal plane and edge sites (see Figure 1). It was recognized many years ago that these sites have vastly different chemical reactivities. For example, the oxidation rate and oxygen chemisorption at the edge sites are much higher than that of the basal plane (33-35). There are reports (36-40) suggesting that the irreversible capacity loss is strongly affected by the relative amounts of basal plane and edge sites. These studies concluded that the edge sites are the more active (catalytic) sites for electrolyte decomposition. Equations [5] and [6] show that Q_{irr} increases with an increase in surface area, however this relationship does not provide insight into the role of basal and edge sites on Q_{irr}. More detailed studies by Chung et al. (36) and Zaghib et al. (37) concluded that the edge sites, despite their low concentration on graphite particles, play a major role in the magnitude of Q_{irr}. Their analyses indicated that reactivity of the edge sites is about 7 times higher than that on the basal plane sites.

Because Li-ion batteries are manufactured in the discharged state (i.e., cells are fabricated with no Li in the carbon electrode), an excess amount of positive electrode material must be used to compensate for the ICL, which reduces the amount of Li that is available for the intercalation or insertion reactions. The actual and theoretical mass ratios (γ) of the active materials in the positive (subscript +) and negative (subscript -) electrodes of Li-ion batteries are defined as (41,42)

$$\gamma_{actual} = m_+/m_- = (\delta_+\varepsilon_+\rho_+)/(\delta_-\varepsilon_-\rho_-) \qquad [7]$$

and

$$\gamma_{theoretical} = (\Delta x C_-)/(\Delta y C_+) \qquad [8]$$

respectively. The parameter m is the mass of active material in the composite electrode (g/cm^2), δ is the electrode thickness (cm), ε is the volume fraction of active material, ρ is the density of active material (g/cm^3), C is the theoretical coulombic capacity of insertion material based on discharged state (mAh/g), and x and y are the stoichiometric coefficients for the negative (e.g., Li $_x$C$_6$) and positive (e.g., Li$_y$Mn$_2$O$_4$) electrodes, respectively. When the ICL and side reactions at the negative electrode are considered, this contribution (C$_{irr}$) yields

$$\gamma_{actual} = (\Delta x C_- + C_{irr})/(\Delta y C_+) \qquad [9]$$

The magnitude of C_{irr} represents the additional capacity needed during the initial formation cycles, and will impact the mass ratio of the active material in the negative and positive electrodes. The additional capacity can be defined in terms of a percent (i) of the reversible capacity, C_-. In other words,

$$C_{irr} = i \, C_- \qquad [10]$$

The relationship between the mass ratio (Equation [7]) and electrochemical parameters (Equation [9]) yields

$$(\Delta x C_- + C_{irr})/(\Delta y C_+) = (\delta_+ \varepsilon_+ \rho_+)/(\delta_- \varepsilon_- \rho_-) \qquad [11]$$

which leads to

$$(\delta_+ \varepsilon_+ \rho_+)/(\Delta y C_+) = (\delta_- \varepsilon_- \rho_-)(\Delta x C_- + C_{irr}) \qquad [12]$$

Equation [12] is useful to compare the properties of different negative electrodes in combination with the same positive electrode. Taking the electrode thickness of the negative electrode, for example, the following equation is derived from Equation [12];

$$(\delta_-)_a = [(\delta_- \varepsilon_- \rho_-)(\Delta x C_- + C_{irr})]_g / [(\varepsilon_- \rho_-)(\Delta x C_- + C_{irr})]_a \qquad [13]$$

where the subscripts a and g refer to the alternative anode and graphite, respectively. Equations [10] and [13] is used here to compare the relative thickness of a graphite electrode to that of an alternative anode in Li-ion cells that contain the same positive electrode. To make this analysis, some of the characteristics of the negative electrodes must be assumed, and representative values are summarized in Table 1. The results are plotted in Figure 6. The thickness of alternative anodes decreases as the irreversible capacity loss increases and reversible capacity increases. This trend is attributed to the fact that the capacity of the positive electrode is fixed. Therefore, when the irreversible capacity loss increases, a greater fraction of the capacity of the positive electrode is consumed in Q_{irr}, and a lesser amount is available to contribute to the reversible capacity of the negative electrode. The consequence is that the alternative anode must be made thinner because of the limited capacity of the positive electrode. Furthermore, the electrode thickness of the alternative anodes is much less than that of graphite, which is assumed to be 100-μm thick. These observations suggest that any gain in reversible capacity that is attained with alternative anodes must be balanced with the minimum electrode thickness than can be readily fabricated. A more sophisticated analysis and improved model would be helpful to determine the optimum combination of positive electrode and alternative anode for Li-ion batteries.

Summary

A number of physicochemical properties play important roles in the electrochemical performance of carbons in negative electrodes for Li-ion batteries.

Examples based on experimental evidence of the relationship between the physicochemical properties of carbon and their impact on electrochemical parameters are presented in Table 2. The table is not intended to be inclusive, but serves as a point for analyzing the role that the physicochemical properties of carbon play on the electrochemical performance of the negative electrodes in Li-ion batteries.

Acknowledgment

Tables

Table 1. Characteristics of negative electrodes.

Parameter	Graphite	Alternative Anode
Electrode thickness (cm)	0.01	variable
Volume fraction	0.36	0.50
Density (g/cm^3)	2.2	5.0
C (mAh/g)	372	400-800
i	0.15	0.05-0.30
x, y	1	1

Table 2. Correlation between physicochemical properties and electrochemical parameters of carbons in Li-ion batteries.

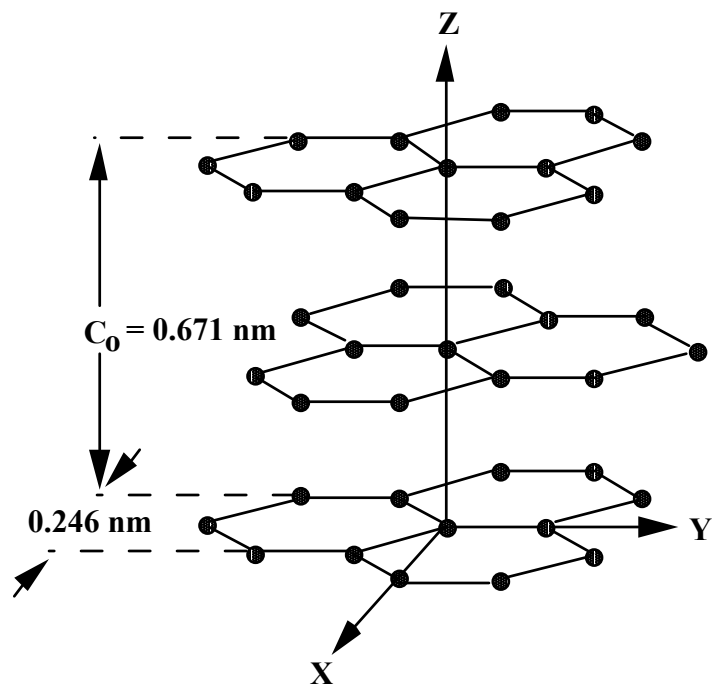| Physicochemical properties	Electrochemical parameters
Particle size - distribution	Li$^+$-ion intercalation/de-intercalation rate Irreversible capacity loss

Particle morphology
    - spherical (3-D)
    - flakes (2-D)
    - fiber (1-D)
	Li$^+$-ion intercalation/de-intercalation rate
	Energy density

Surface area - microporosity	Irreversible capacity loss

Degree of graphitization
    - d(002) spacing
    - L_c, L_a
	Reversible capacity
	Charge/discharge potential profile

Fraction of edge/defect sites - crystallinity	Irreversible capacity loss

Electrode parameters
    - type and morphology of carbon
    - fraction of carbon
    - tap density
    - thickness
	Li$^+$-ion intercalation/de-intercalation rate
	Energy density
	Impedance

References

1. K. Kinoshita, <u>Carbon Electrochemical and Physicochemical Properties</u>, Wiley and Sons, New York, p. 20 (1988).

2. W. Hess, C. Herd in <u>Carbon Black Second Edition, Revised and Expanded</u>, J. Donnet, R. Bansal and M. Wang, eds., Marcel Dekker, New York, USA, p. 89 (1993).

3. I. Spain, in <u>Chemistry and Physics of Carbon</u>, Vol. 16, P. Walker and P. Thrower, eds., Marcel Dekker, New York, p. 119 (1981).

4. P. Delhaès, F. Carmona, in <u>Chemistry and Physics of Carbon</u>, Vol. 17, P. Walker and P. Thrower, eds., Marcel Dekker, New York, p. 89 (1981).

5. E. Dannenberg, in <u>Kirk-Othmer: Encyclopedia of Chemical Technology</u>, Vol. 4, Wiley and Sons, New York, p. 631 (1978).

6. J. Maire and J. Mering, in <u>Proceedings of the Fourth Conference on Carbon</u>, Pergamon Press, New York, p. 345 (1960).

7. S. Megahed and B. Scrosati, J. Power Sources, 51, 79 (1994).

8. J. Besenhard and M.Winter, in <u>Ladungsspeicherung Doppleschicht</u>, Tagungsband, W. Schmickler, ed., Ulmer Elektrochem. Tage, 2nd, 1994, Universitaetsverlag, Ulm. Germany, p. 47 (1995).

9. J. Tarascon and D. Guyomard, Electrochim. Acta, **38**, 1221 (1993); D. Guyomard and J. Tarascon, Solid State Ionics, **69**, 222 (1994).

10. S. Hossain, in <u>Handbook of Batteries</u>, Second Edition, D. Linden, ed., McGraw-Hill, Inc., New York, p. 36.1 (1995).

11. K. Kinoshita, in <u>New Trends in Electrochemical Technology: Energy Storage Systems for Electronics</u>, T. Osaka and M Datta, eds., Gordon and Breach Science Publishers, Reading UK, p. 193 (2000).

12. M. Endo , C. Kim, K. Nishimura, T. Fujino and K. Miyashita, J. Power Sources, **38**, 183 (2000).

13. A. Satoh, N. Takami and T. Ohsaki, Solid State Ionics, **80**, 291 (1995).

14. M. Wakihara, Functional Materials, **14**, 5 (1994).

15. T. Tran, L. Spellman, W. Goldberger, X. Song and K. Kinoshita, J. Power Sources, **68**, 106 (1997).

16. W. Xing, J. Xue, T. Zheng, A. Gibaud and J. Dahn,   J. Electrochem. Soc., **143**, 3482 (1996).

17. Y. Liu, J. Xue, T. Zheng and J. Dahn, Carbon, **34**, 193 (1996).

18. T. Zheng, W. Xing and J. Dahn,   Carbon, **34**, 1501 (1996).

19. P. Zhou, P. Papanek, R. Lee, J. Fscher and W. Kamitakakara, J. Electrochem. Soc., **144**, 1744 (1997).

20. J. Dahn, W. Xing and Y. Gao,   Carbon, **35**, 825 (1997).

21. A. Mabuchi, K. Tokumitsu, H. Fujimoto and T. Kasuh, J. Electrochem. Soc., **142**, 1041 (1995).

22. A. Mabuchi, H. Fujimoto, K. Tokumitsu and T. Kasuh, T., J. Electrochem. Soc., 142, 3049 (1995).

23. K. Tokumitsu, A. Mabuchi, H. Fujimoto and T. Kasuh, J. Electrochem. Soc., **143**, 2235 (1996).

24. Y. Matsumura, S. Wang and J. Mondori, Carbon, 33, 1457 (1995).

25. S. Wang, Y. Matsumura and T. Maeda, Synth. Met., **71**, 1759 (1995).

26. K. Sato, M. Noguchi, A. Demachi, N. Oki and M. Endo, Science, **264**, 556 (1994).

27. K. Sato, M. Noguchi, A. Demachi, N. Oki, M. Endo and Y. Sasabe, in Proceedings of International Workshop on Advanced Batteries (Lithium Batteries), February 22-24, 1995, Osaka, Japan, Science and Technology Agency of Japan, Tokyo, Japan, p. 219 (1995).

28. S. Flandrois and B. Simon, Carbon, **37**, 165 (1999).

29. H. Fujimoto, A. Mabuchi, K. Tokumitsu and T. Kasuh, Carbon, **32**, 193 (1994); **32**, 1249 (1994).

30. R. Yazami, Electrochim. Acta, **45**, 87 (1999).

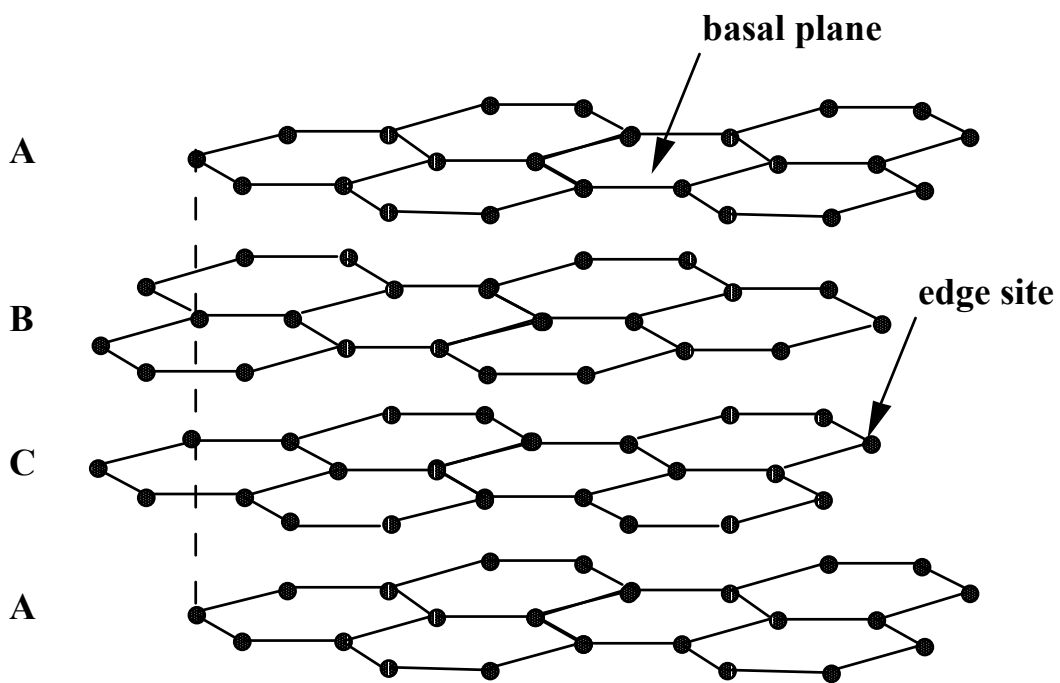31. F. Joho, B. Rykart, A. Blome, P. Novak, H. Wilhelm and M. Spahr, J. Power Sources, **97-98**, 78 (2001).

32. T. Tran, B. Yebka, X. Song, G. Nazri, K. Kinoshita and D. Curtis, J. Power Sources, **85**, 269 (2000).

33. L. Radovic, P. Walker and R. Jenkins, Fuel, 62, 849 (1983).

34. N. Laine, F. Vastola and P. Walker, J. Phys. Chem., **67**, 2030 (1963).

35. M. Coltharp and N. Hackerman, J. Phys. Chem., **72**, 1171 (1968).

36. G-C. Chung, S-H. Jun, K-Y. Lee and M-H. Kim, J. Electrochem. Soc., **146**, 1664 (1999).

37. K. Zaghib, G.Nadeau and K. Kinoshita, J. Electrochem. Soc., **147**, 2110 (2000).

36. M. Winter, P. Novak and A. Monnier, J. Electrochem. Soc., 1**45**, 428 (1998).

39. D. BarTow, E. Peled and L. Burstein, J. Electrochem. Soc., **146**, 824 (1999).

40. O. Yamamoto, Y. Takeda and N. Imanishi, in <u>Proceedings of the Symposium on New Sealed Rechargeable Batteries and Supercapacitors</u>, B. Barnett, E. Dowgiallo, G. Halpert, Y. Matsuda and Z. Takehara, Editors, PV 93-23, p. 302, The Electrochemical Society, Inc., Pennington, NJ (1993).

41. P. Arora, M. Doyle and R. White, J. Electrochem. Soc., **146**, 3543 (1999).

42. P. Arora, R. White and M. Doyle, J. Electrochem. Soc., **145**, 3647 (1998).

Figure Captions

1. Model of graphite structures.

2. Schematic representation of the potential profiles for carbon electrodes with Li^+ ions intercalated at constant current.

3. Dependence of the reversible capacity (Q_{rev}) as a function of the d(002) spacing of carbon.

4. Relationship between the reversible capacity and irreversible capacity loss of graphite in $LiClO_4$ in EC-DMC (1:1). Solid line, data from Yazami (30).

5. (A) Dependence of irreversible capacity loss on the BET surface area of natural graphite in $LiClO_4$ in EC-DMC (1:1). (B) Plot of ICL versus BET surface area from published data for various carbons (32).

6. Comparison of the thickness of graphite electrode and alternative anode.

Z

$C_o = 0.671$ nm

0.246 nm

Y

X

**Hexagonal
graphite**

basal plane

A

B

edge site

C

A

**Rhombohedral
graphite**

Electrolyte decomposition

Gas evolution

Graphitic carbon

Amorphous carbon

Staging

Potential (V)

Capacity (mAh/g)

Reversible capacity (mAh/g) vs Irreversible capacity loss (mAh/g)

Assumptions:
Carbon electrode thickness = 100 micron
Vol. fraction active matl.: C = 0.36, alt. anode = 0.5

Density: C = 2.2 g/cm^3, alt. anode = 5 g/cm^3
Irrev. capacity loss (%): C = 15%
Positive electrode: constant

Irreversible capacity
(alt. anode)

- 5%
- 10%
- 20%
- 30%